# Limitations to SAR interferometry due to instrument, climate or target geometry instabilities

**D. Massonnet**

Centre National d'Etudes Spatiales
18, avenue Edouard Belin
31055 Toulouse Cedex, France

## ABSTRACT

Now that SAR interferometry has demonstrated its capabilities in small displacements detection as well as in digital elevation model (DEM) derivation, new applications demand longer scenes and better precision, over longer time periods. We show an example of such demanding applications.

The paper exposes the technical problems to this goal, such as the instrumental limitations which we characterize, the limitations brought by meteorological problems, of which we give two very different and well documented examples and the behaviour of the targets under various orbital conditions and separation in time, which affects the phase preservation, or coherence.

The contributions of various artifacts can be identified using a simple pair-wise logic which we present. Some hypotheses on the shape of the coherence function versus time are made and backed by various examples.

The special case of volume scattering is addressed, and the question of how special filters aimed at improving the coherence in that case could threaten the operational status of SAR interferometry.

## BACKGROUND

SAR interferometry has demonstrated its capability to produce large scale digital elevation models or to detect small displacements of various origins, such as surface deformation produced by a large earthquake (ref. 1), a landslide (ref. 2), a smaller earthquake or fault slip as small as 2 cm (ref. 3). Other studies detected the effect of tides on glaciers (ref. 4) or phase surface changes (ref. 5).

At the radar processing group of CNES we developed an automated differential interferometry software tool (ref. 6), which is used for the production of topographic models (ref. 7) as well as for new scientific developments in cooperation with field specialists.

This software tool works from a pair of radar raw data and a digital elevation model (DEM). If the DEM is not available we substitute the geoid or the ellipsoid to it. Otherwise, the topographic contribution is automatically retrieved from the interferogram, which can be placed into any map coordinates or kept in slant range geometry. The tool, based on the application of the digital elevation model elimination method (ref. 8), produces a result which can be used to increase the accuracy of an existing DEM (ref. 9) through the analysis of residual fringes or to give information on possible displacements. The tool produced results with ERS-1 as well as J-ERS. The DEM is used at four critical steps of the processing:

– it predicts the deformation between the images using preliminary orbits, including the small deformation due to topography. This predicted deformation is compared to the actual deformation obtained from local correlations. Two constant offsets (range and azimuth) generally suffice to characterize the differential comparison. This method is equivalent to comparing the whole images by correlation to obtain only two constant offsets. The quality of the result reflects this huge signal to noise ratio; the accuracy on the offsets is on the order of 3% to 5% of a pixel size in both directions.

– it allows the production of a fake amplitude image, which is then compared to one of the radar images and gives, by correlation, the absolute position of the images with an accuracy of a fraction of the DEM cell size.

– it selects, during data fusion, the optimal slope dependent finite (at most five range pixels) impulse response fil-

ter which maximizes the coherence, thus contributing to the quality of the fringes.

– it allows the prediction of the topographic and orbital fringe pattern of the pair, which we subtract from the interferogram, creating the differential product. This product is map corrected most of the time to the DEM (with the same cell size) and is made of three channels; a combined serial multilook image of the amplitude, a phase from the complex averaging on the cell size and a coherence computed on the cell size.

The notion of altitude of ambiguity is convenient to qualify the orbital configuration of a given interferometric pair. It is equal to the change of elevation which produces a change of one topographic fringe in the interferogram. The worse orbital configurations give altitudes of ambiguity of slightly less than ten metres in the case of ERS-1. We obtained usable results with 8.5 metres on very flat areas. In such optimal cases, the estimated accuracy of the DEM derived from the interferogram is of the order of one metre over the 10000 sq. km. of the scene. We had to confirm this value of accuracy using several pairs in order to eliminate the scene dependent artifacts we describe later.

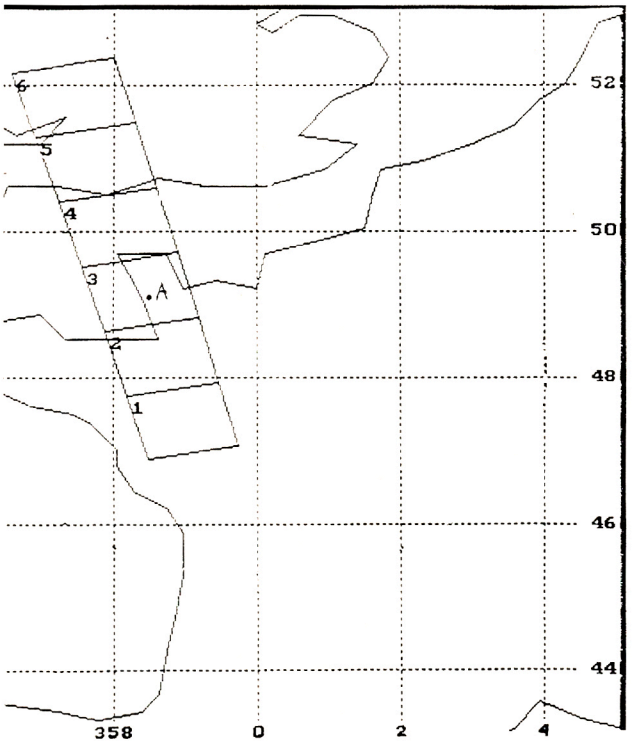


*Figure 1 - The tidal load project intends to measure the response of a coast to the weight of the water rushing toward the Baie du Mont St Michel during high tides*

## NEW DEMANDING APPLICATIONS

Conventional applications of differential interferometry or DEM computation deal with a typical scene size or less (i.e. less than 100 km). The displacements amount to 10 cm to several meters and develop over at least one square kilometre. We tried to go further with the study of the Landers earthquake, where the large extension of the site (300 km) required very accurate orbit modelling. However, the displacements to be measured were still very large. New applications may be much more demanding in terms of scene length and calibration accuracy.

An example where interferometry would be pushed forward in terms of performance is the measurement of local tidal loads on the Earth's crust, caused by ocean tides. We plan to study the effect of such a loading on the Cotentin (Normandy, France) in cooperation with GRGS. For this purpose we should be able to study a 600 km long scene for the detection of centimetre sized phenomena (figure 1).

This urges us to place a high priority on the study of the specific artifacts which could make such applications difficult. We already identified two of them, which will be described now. Of course, the new application still demands a high level of coherence, like any interferometric operation, and we will share our experience on this topic.

## LIMITS DUE TO THE INSTRUMENT

Clock instabilities were discovered (ref. 10) using a very long interferometric strip, acquired during orbits 1014 and 1100 (six days apart: 25th of September and 1st of October1991, 1 am local time), when ERS-1 was in commissioning phase. The length of the strip is 3000 km of which half a million formats were processed (see map as figure 2). These orbits are interesting because they present a natural attenuation of all the phenomena which usually create the interest of interferometry. The baseline is small; at the beginning of the data take, the horizontal shift is 65.5 m and the vertical shift is 12.5 m, while at the end of the data take, the horizontal shift is -11.5 and the vertical shift is 8 m (the scene presents therefore an orbit crossing). The altitude of ambiguity ranges from 120 m in Crimea to -327 m in Finland. The change of sign is due to the orbit crossing somewhere above the Gulf of St Petersburg, where the altitude of ambiguity is infinite. These rather small baselines are associated with the moderate altitudes of the regions laying between southern Ukraine and northern Finland.

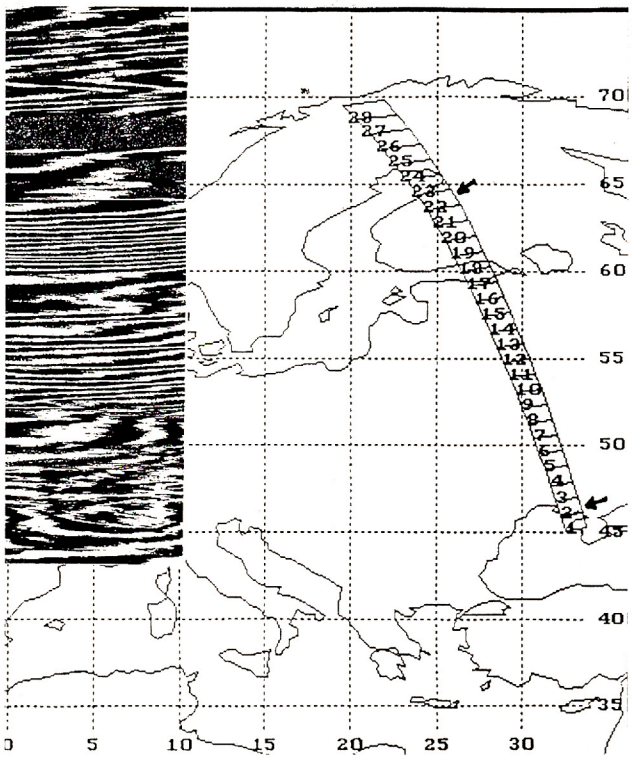


*Figure 2 - Map of the long interferometric segment used in the discovery of clock artifacts in ERS-1*

Several groups of fringes can be observed where we would expect no fringe from conventional causes and only a few fringes from the worst expected atmospheric propagation change. Furthermore, these fringes are clearly linked to the pulse lines. The effect is consistent with a time dependent linear error of the carrier frequency of ERS-1, f, whose nominal value is:

$$\mathbf{f_0 = 5.3\ GHz}$$

thus:

$$\mathbf{f = f_0 + \alpha t}$$

**t** being the time and $\alpha$ being the frequency rate, expressed in Hertz per second or $s^{-2}$. The round trip flight time to a given target, whose closest range to the radar is $\mathbf{R_1}$, creates a delay $\delta_1$ equal to:

$$\delta_1 = \frac{\mathbf{2R_1}}{\mathbf{c}} \text{ (c: light velocity)}$$

Assuming an ERS-1 image ranges between 820 km and 870 km, $\mathbf{d_1}$ ranges between 5.47 millisecond and 5.8 millisecond. Due to this delay, the target is out of phase by:

$$\phi_1 = \int_{\mathbf{nPri}}^{\mathbf{nPri} + \delta_1} (f_0 + \alpha t)\, dt = (f_0 + \alpha\, n\, Pri)\, \delta_1 + \alpha \frac{\delta_1^2}{2}$$

where **Pri** is the time interval between pulses and **n** the number of pulses since the frequency perturbation began. $\phi$ is expressed as a number of cycles. The interferometric acquisition requires the target to be illuminated a second time by the radar, at range $\mathbf{R_2}$, creating a delay $\delta_2$. The target is out of phase by:

$$\phi_2 = (\mathbf{f_0} + \Delta_{12})\, \delta_2$$

where we assume that the frequency is stable during the second pass but tuned at a slightly different level. Such a different value could be due to a slight change $\Delta_{12}$ in the clock of the same satellite or to a more systematic offset if the second pass is made by another satellite of the same kind (i.e. ERS-1/ERS-2): $\mathbf{f = f_0 + \Delta_{12}}$. We have access only to the difference $\phi_2 - \phi_1$ of the phase variation, since we must get rid of any phase term linked to the physical properties of the targets or to its internal geometric organization.

$$\phi 2 - \phi 1 = f_0\, (\delta_2 - \delta_1) + \Delta_{12}\delta_2 + \alpha\, \mathbf{n\ Pri}\ d1 - \alpha \frac{\delta_1^2}{2}$$

The term $f_0\, (\delta_2 - \delta_1)$ is exactly what we expect from the interferometric measurement. The term $\Delta_{12}\delta_2$ creates non Euclidean fringes parallel to the satellite track. A change of $\Delta_{12}$ = **10 kHz** would create **3.3** such fringes across the swath of ERS-1, where $\delta_2$ is assumed to change by 0.33 millisecond (round trip flight time for 50 km of range). Such fringes across the swath are to be expected during ERS-1/2 operations if the clocks are not tuned on the same frequency and would be easily cured by preliminary calibration of the clocks by segments acquired in the visibility of a laser ranging station. This way we could exclude a contribution by an orbital error, which may show the same signature (fringes across the swath). We will conduct such a calibration early in the life of ERS-2 as part of our investigation.

The term $\alpha$ **n Pri** $\delta_1$ creates the kind of artifact linked to the line we observe. Values of up to **82** Hertz per second have been observed. The last term $\alpha \frac{\delta_1^2}{2}$ is negligible. The change of frequency of the ERS-1 clock deduced from the first group of artifactual fringes amounted to **2500 Hz**. Each fringe perpendicular to the track is the signature of a **180 Hz** clock frequency change.

**Consequences on geometric accuracy**

A phase ramp in azimuth affects the geometry of the image. If **Fps** is the number of fringes per second expe-

rienced by the image in azimuth; **B** the azimuth bandwidth expressed in a number of azimuth pixels; **Prf** the pulse repetition frequency and **Off** the offset from zero Doppler in the raw data, we should observe an azimuth displacement of:

$$N = \frac{\mathbf{Off\ B\ Fps}}{\mathbf{Prf}}$$

N being expressed as a number of azimuth pixels (usual values for other terms are: **B = 1350, Prf = 1680 Hz** and **Off = 0.25**). The loss of quality of the interferogram, due to mis-registration, becomes severe if **N > 0.5**. This would be the case if: **Fps < 2.5**.

## LIMITS DUE TO METEOROLOGICAL CONDITIONS

Any change in the propagation conditions in the atmosphere presents a very different signature than topographic or instrumental artifacts. The scene where the problem occurred is identified because all the interferometric pairs to which it participated are affected by the artifact with a constant level. In this, it is similar to the instrumental clock artifact, but unlike the latter, it is not linked to the pulse lines and its amplitude is unlikely to reach more than a few fringes. Once the faulty image has been identified, one can check, knowing the exact time of the data take, the meteorological conditions at that time.

A first example of atmospheric propagation change can be found in the July 3 image acquired in Southern California. A kidney-shaped depression, with a depth of one fringe, or 28 mm, and a size of 25 km (N-S) by 10 km (W-E), can been seen on each interferogram formed with the July image. Since these interferograms show altitudes of ambiguities ranging from 17 m to 250 m, a topographic error cannot be invoked as it would have produced different numbers of fringes. A ground geophysical change cannot be the explanation, because interferograms spanning a larger time period than those where the kidney is visible do not show it. Such a ground change should have been reversible, which is unlikely. Besides, no corresponding seismic activity nor water withdrawal can be found in this place and time (ref. 3). A propagation problem occurring at 18:28:36.4 UT on July 3 1992 is the only explanation. Neither the 17:01 meteorological image nor the 19:31 image show any clouds, in visible or infra-red. This is a "nice weather" propagation change. We are in the process of checking whether GPS data could decide if the problem is tropospheric or ionospheric. The identification of the image responsible allows us to say that the waves travelled **faster** in the kidney than in a standard atmosphere.

Similarly, the image of August 27 1993, 18:28 UT, shows several 5 to 10 km wide irregular, circular patterns, amounting to up to three fringes (figure 3), which are clearly identified as propagation problems using the above logic. Unlike the previous example, the meteorological image of 19:31 shows a chain of small circular clouds which are not yet formed in the 17:01 image (figure 4). This indicates that the fringes are due to tropospheric turbulence, possibly linked to the formation of thunderstorm clouds. Further investigation is being conducted on these phenomena.

Since atmospheric propagation changes are likely to produce azimuth phase gradients similar or worse than the

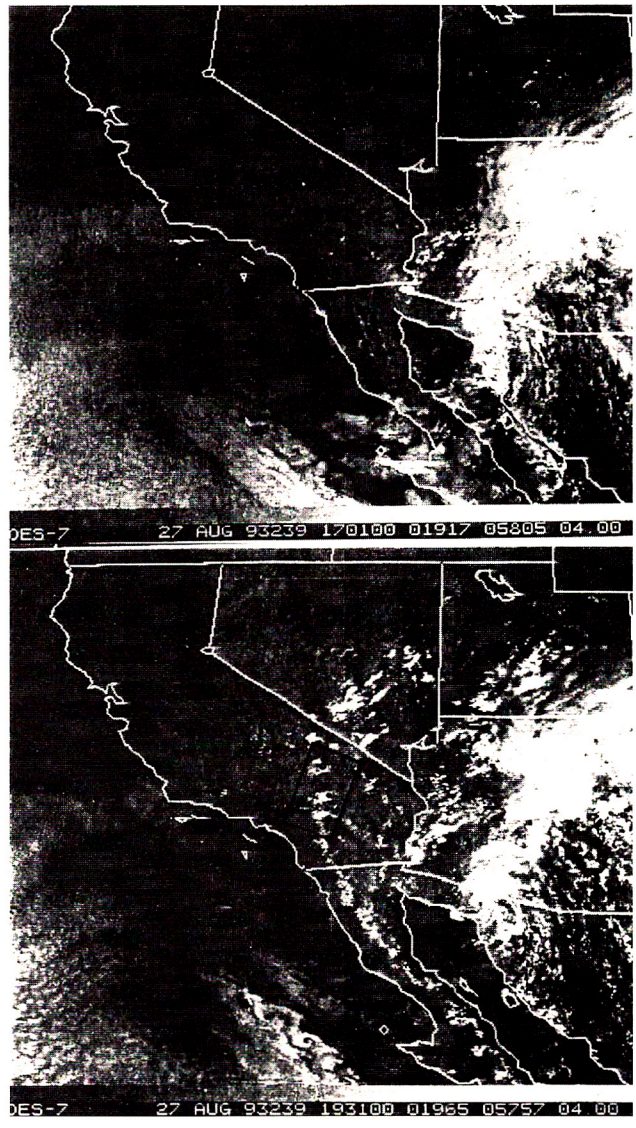


*Figure 3 - Fringe patterns associated with clouds in Southern California*

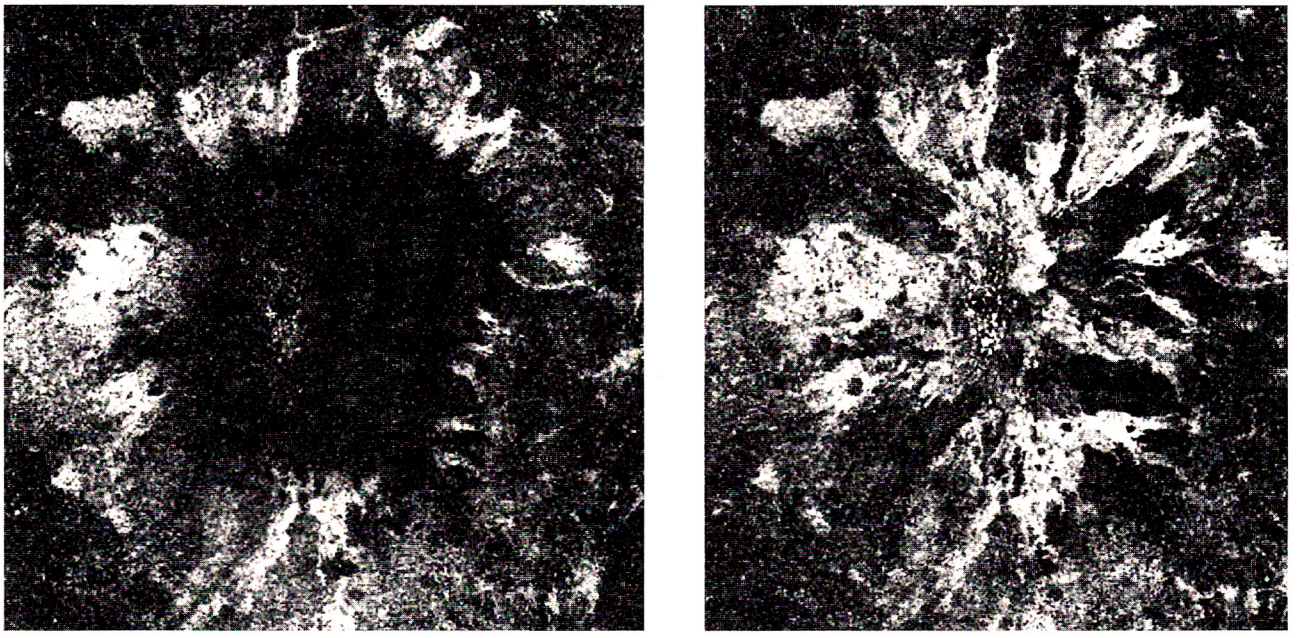

*Figure 4 - Meteorological images taken before and after the radar image believed to have been affected by propagation errors*

ones caused by internal clock drift. We may expect problems in the geometry of the final image, which may be of critical importance in regard of interferometric co-registration. In the case of the August 27 image, we observe a phase gradient reaching **Fps = 3** (one fringe created in two kilometers) with **Off = 0.2**, which caused a mis-registration of about **0.6** azimuth pixel, close to causing the loss of the interferometric effect.

## LIMITS DUE TO THE COHERENCE LOSSES

An advantage of the coherence losses, when compared to the other causes of interferometric misbehaviour, is that they do not create biases in the measurement. A coherence loss is typical of less and less readable fringes till they are changed into equally distributed noise. This change never creates a wrong measurement although the standard deviation keeps climbing.

A critical knowledge for the future of SAR interferometry is the behaviour of the coherence, which measures the quality of phase preservation, with time and surface types. Generally accepted models (ref. 11) assume a linear loss of coherence with time with a slope depending on surface type. Although it is clear that the general trend of coherence versus time could only be a decrease, we observed clear examples of coherence rebuilding with time.

In particular, on the test site of Mount Etna, which we study within ESA's fringe group, we observed a higher coherence between orbits 6286 and 9292, than between orbits 6787 and 8290. This significantly higher coherence cannot be attributed to a better orbital configuration, since the altitude of ambiguity was worse (18 m) for the first pair than for the second (41 m). Permanent surface changes are excluded because the 210 day time interval of the first pair includes totally the 105 day time interval of the second pair (see the two coherence map as figure 5).

We have no clue as to what could cause a reversible surface state, but soil moisture appears to be a very likely candidate, as it can be restored to its initial value. The coherence of a pair could also be spoiled by bad conditions (for instance high winds) applied to one of the images of the pair.

The summit of Mount Etna is also subject to coherence changes for which frost could be invoked (similar results have been observed by JPL scientists in the Aleutians).

We have two beliefs concerning the behaviour of coherence, which we did not prove completely but which drove our new developments:

– coherence reaches a lower threshold which corresponds to the contribution of hard targets in the terrain. We observed fringes on data separated in time by more than two years. The final quality of the fringes depends on the value of this contribution. It is obviously very high in a desert environment, but seems to exist in any environment with the exception of purely agricultural areas. We developped

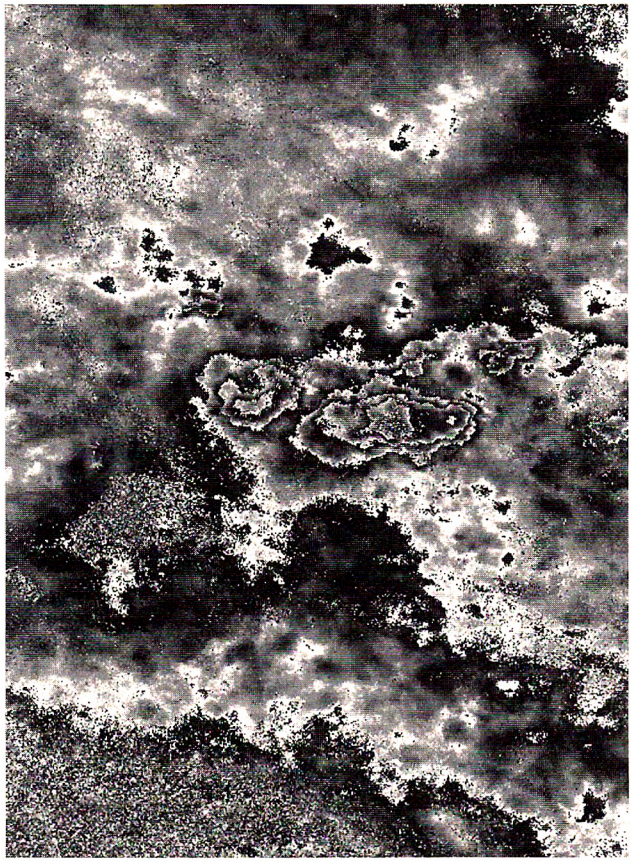

*Figure 5 - Comparison of the coherence of two interferograms acquired on Mount ETNA. The coherence is higher in the square where the digital elevation exists because the dense fringe pattern associated with topography blurs the coherence assessment. The interesting aspect of this comparison is the lower coherence of the "best" image, as explained in the text. The Mount ETNA is analyzed within ESA's fringe group. The processing has been performed by A. Arnaud, a PhD student co-sponsored by ANRT and CISI, working at CNES*

a program which identifies the similarity of each point with its immediate neighbours within a time series of interferograms. This program gives good visual improvements which are difficult to quantify, since the result eliminates the points which are not recognized as coherent. Thus, we cannot reconstruct a coherence function comparable to the initial one

– volume scattering has a major impact on coherence. In Southern California, we observed more severe coherence losses on forested areas, as compared to areas where the terrain slopes were similar. However, the situation is not hopeless, as data acquired much later, but with a better orbital configuration, showed an almost complete recovery of the coherence losses. This suggests that targets showing volume scattering are more demanding in terms of orbital repetition than surface targets. As a consequence, the filters we use for interferometric scene matching, which were empirically optimized for surface targets using only the local terrain slope as input, could be optimized with a target dependence. Early results show an improvement in some volume scattering areas which is balanced by a degradation in the previously coherent areas. Again, we cannot yet quantify the global output since we refuse to consider local improvements (any filter improves the coherence provided it is used "very locally"!). Another question is the ability of SAR interferometry to remain operational and automated if target dependent filtering is required in volume scattering areas.

## CONCLUSIONS

The extension of SAR interferometry to large scale mission, either scientific (such as tidal loads assessment) or industrial (such as global Earth DEM) create new challenges. The production of interferograms can be automated and conducted on a very large scale, and is likely to become a standard receiving station product. But the threat comes from the interpretation of such a vast amount of data.

Some artifacts due to improper instrument specification (no instrument has been specified for interferometry so far) will be easily solved by a moderate amount of technology in the next generation radar satellites.

Propagation problems are much more difficult to deal with and produce up to three fringes in C-band. Tropospheric as well as ionospheric problems may be involved. A first priority is to decide whether these problems could be solved using existing meteorological data.

The coherence was shown to survive, in some cases, for two years. Far from being a regular decreasing function of time, it appears quite chaotic. In particular, it can be restored with time, in some cases, and is likely to reach a "hard target threshold" where it could stabilize for years. The coherence is clearly dominated by geometric conditions, well known with surface targets, but more difficult to assess in volume scattering conditions. Preliminary results show that a volume scattering target is more demanding in terms of orbit repetition. Special filters matched to specific volume scattering targets are promising, but could threaten the operational status of SAR interferometry by introducing non-standard products.

It is clear that interferometry brings a revolution into several fields, and especially in geophysics. This remains true but it will not be an easy revolution. There are several dif-

ficulties to be solved before proposing global mission concepts. This is the main axis of work at the radar processing group of CNES nowadays.

## REFERENCES

(1) Massonnet D., Rossi M., Carmona C., Adragna F., Peltzer G., Feigl K. & Rabaute Th., The displacement field of the Landers earthquake mapped by radar interferometry, Nature vol 364 n° 6433, 8 July 1993.

(2) Achache J., Fruneau B. *et al.*, 1993, Surface displacements mapping of the Saint-Etienne-de-Tinée landslide using SAR interferometry, EOS supplément Oct. 26, 74, p. 67.

(3) Massonnet D., Feigl K., Rossi M. & Adragna F., Radar interferometric mapping of deformation in the year after the Landers earthquake, Nature vol 369, 227-230, 19 May 1994.

(4) Goldstein R.M., Engelhardt H., Kamb B. & Frolich R.M., Satellite Radar Interferometry for Monitoring Ice Sheet Motion: application to an Antartic Ice Stream, Science, 262, pp. 1525-1530, 1993.

(5) Gabriel A.K., Godstein R.M. & Zebker H.A., 1989, Mapping small Elevation Changes over large Areas: differential radar interferometry, Journal of Geophysical Research 94, pp. 9183-9191.

(6) Massonnet D., Giving an Operational Status to SAR Interferometry, ERS-1 Pilot Project Workshop Toledo (06-94), pp 379-382.

(7) Renouard L. & Perlant F., Comparison of the SPOT DEM and the ERS interferometric DEM, 14th Earsel Symp. Topography from Space, Goteborg, 8-10 june 1994.

(8) Massonnet D., Etude de principe d'une détection de mouvements tectoniques par radar, CT/PF/TI/AS n° 326 (CNES internal memo.), 1985.

(9) Adragna F., SAR interferometry applied to DEM generation at CNES, 14th Earsel Symp. Topography from Space, Goteborg, 8-10 june 1994.

(10) Massonnet D., Vadon H., ERS-1 Internal Clock Drift Measured by Interferometry, IEEE (TGARS) vol 33, n° 2, 1-8 (03-1995).